Direct Growth of Single-Walled Carbon Nanotube Films and Their Optoelectric Properties

ARTICLE *in* THE JOURNAL OF PHYSICAL CHEMISTRY C · JULY 2009

Impact Factor: 4.77 · DOI: 10.1021/jp8114463

6 AUTHORS, INCLUDING:

Huafeng Wang
Tokyo University of Science
17 PUBLICATIONS **160** CITATIONS
SEE PROFILE

Takahiro Maruyama
Meijo University
65 PUBLICATIONS **346** CITATIONS
SEE PROFILE

Sakae Inoue
Meijo University
23 PUBLICATIONS **710** CITATIONS
SEE PROFILE

Yoshinori Ando
Meijo University
186 PUBLICATIONS **5,880** CITATIONS
SEE PROFILE

Direct Growth of Single-Walled Carbon Nanotube Films and Their Optoelectric Properties

Huafeng Wang,*,† Kaushik Ghosh,† Zhenhua Li,‡ Takahiro Maruyama,† Sakae Inoue,† and Yoshinori Ando†

21st COE Program "Nano Factory", Department of Materials Science & Engineering, Meijo University, Shiogamaguchi 1-501, Tenpaku-ku, Nagoya 468-8502, Japan, and Department of Mechanics, Zhejiang University, Hangzhou 310027, China

Received: December 28, 2008; Revised Manuscript Received: April 29, 2009

We introduce a new method to synthesize semitransparent continuous single-walled carbon nanotube (SWNT) films by the arc discharge process. Our analyses indicate that the directly grown films are weaved by long and high-quality SWNTs, in which a considerable amount of metallic tubes have been identified. Because of this unique continuous network structure, the sheet resistance of a 150 nm thick film with a transmittance higher than 77% is 117 Ω/□. Moreover, the as-grown film shows an excellent field emission property with low turn-on (E_{to} = 0.4 V/μm) and threshold fields (E_{th} = 1.4 V/μm) corresponding to the emission current density of 0.1 μA/cm^2 and 1 mA/cm^2, respectively.

Single-walled carbon nanotubes (SWNTs) have attracted an extensive focus because they have tremendous potential applications. The unique 1D structure of SWNTs makes them a good subject to perform theoretical and experimental studies.[1] During the extensive research, it has been found that individual tubes can be used to make various devices.[2,3] The pioneering work was done by Avouris et al. to fabricate field effect transistors.[2] Then the application of individual tubes for chemical sensors has been developed.[4] Recently, a lot of effort has been devoted to growing aligned individual nanotubes on sapphire or quartz substrate.[5,6] It is quite difficult to synthesize SWNTs with uniform diameter, structure, and chirality in a repeated number of reactions; hence, the property of devices cannot be controlled in a unique direction.

On the other hand, the properties of network structures or films assembled by SWNTs are determined from thousands of tubes rather than an individual one, which will lead to a controllable performance of the bulk material.[7] This technique has been applied to various devices, such as sensors,[8] organic light-emitting diodes (OLED), anodes, etc.[9,10] Continuous SWNT film is not only optically transparent but also electroconductive, which could be a potential complement to indium tin oxide (ITO) glass. Moreover, the SWNT itself has a better emission performance that may lead to the application in field emission display.[11] To realize its potentiality, it is very necessary to find the suitable way to fabricate and reproduce homogeneous films. On the basis of this consideration, several methods, including the drop-drying solution method, Langmuir−Blodgett deposition, solution casting, vacuum-filtering, solid-state process by drawing film from carbon nanotube (CNT) forest, and chemical vapor deposition (CVD) process, have been developed so far.[12−17] The solution-based method to prepare films demonstrated that the arc discharge grown nanotubes are overwhelmingly better than HiPCO (high-pressure CO conversion) nanotubes in all of the critical aspects, including the surface roughness, sheet resistance, and transparency.[10,18] The method of arc discharge has been widely used to prepare SWNTs for its good product quality and ease of fabrication. However, this technique has not yet been reported on the direct growth of SWNT thin films.

In this paper, we report a new direct and quick method to synthesize continuous SWNT films by the arc discharge process. Moreover, without destroying the crystallinity and homogeneity of the as-grown films, we have purified the samples by a two-step purification process. Our experiments indicate that the film made by this method can be directly used as a field emission cold cathode without any tedious treatment and shows an excellent emission performance. The optoelectric properties of films have also been studied in this context.

The SWNT films were directly produced by the dc arc discharge method.[19] The anode and cathode were vertically installed at the center of a water-cooled stainless steel chamber. The anode was a carbon rod (square, 6.5 mm × 6.5 mm) with a homogenously doped Fe catalyst (1 atom %), and the cathode was a pure carbon rod (diameter, 10 mm). During arc discharge, the distance between the two electrodes was kept constant. Two graphite plates (diameter, 150 mm) used to collect films were fixed on the anode and cathode. The arc discharge was performed under a mixture of H_2 and Ar with a total pressure of 200 Torr. After arc evaporation, the SWNT film was peeled off the graphite plate.

Thereafter, we performed a two-step purification process (heating, followed by HCl treatment) to remove impurities, such as amorphous carbon and catalyst particles. Heat treatments were carried out in open air under various temperatures, and then the films were rinsed in HCl solution (37%) for 24 h. The systematic studies of heating temperatures on the as-grown films were performed to obtain the optimal oxidation temperature. After purification, the films were washed by deionized water or ethanol several times to remove adsorbed HCl. Scanning electron microscopy (SEM, Topcon ABT-150F), transmission electron microscopy (TEM, Hitachi H-7000), high-resolution transmission electron microscopy (HRTEM, JEOL JEM-3100FEF), thermogravimetric analysis (TGA, SHIMADZU

* Corresponding author. Phone: +81-(0)52-838-2409. Fax: +81-(0)52-832-1170. E-mail: wanghf@ccmfs.meijo-u.ac.jp.
† Meijo University.
‡ Zhejiang University.

10.1021/jp8114463 CCC: $40.75
Published on Web 06/11/2009

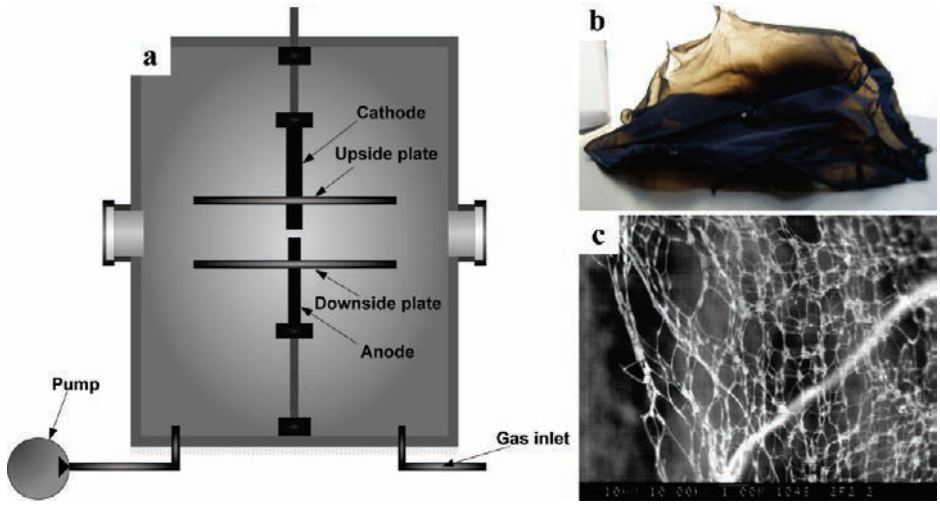

Figure 1. (a) Setup of arc discharge apparatus. (b) Macroscopic image of as-grown freestanding film. (c) SEM image of SWNT bundle network.

DTG-60), and Raman spectroscopy equipped with several lasers (514, 633, and 785 nm) were used to characterize the SWNT films.

For the measurement of film thickness, slices of films were transferred onto quartz substrates and densified by ethanol. Scanning probe microscopy (SPM) was performed at the step edge to determine the thickness of films. The transmittance measurements were carried out on a UV−vis spectroscope (Hitachi U-3500) with a wavelength range from 250 to 900 nm, and the transmittance in the visible range was determined at a wavelength of 550 nm. The sheet resistances of the films was measured by a two-probe method, where the silver adhesive (DOTITE D-500) was used to make good contact. To minimize the effect of contact resistance during measurement, a 10 V potential was applied between the two probes. The power source was supplied by ADVANTEST T6240A, and data were recorded in the ADVANTEST R6452A system.

The films pasted on quartz substrates were directly used as the cathodes of field emission. The distance between the two electrodes was kept at 500 μm. The experiment was carried out with a chamber pressure of 1×10^{-6} Torr, and data were recorded by the ADVANTEST TR8641 system.

To obtain controlled SWNT films using the arc discharge method, there exist several crucial points, the setup of evaporation apparatus, catalysts, and atmospheres. Compared to normally used apparatus, two graphite plates were fixed on the anode and cathode during the arc evaporation (Figure 1a). When the arc was ignited, a high-temperature zone at the core of the arc was formed and the buffer gas driven by heat convection began to flow. Simultaneously, we observed that layers of the SWNT network originated from the center of the arc zone, spread out on the surface of the upside of the graphite plate under buoyancy from convection of buffer gas, and layer-by-layer piled up to form freestanding films. These two graphite plates were used to control the convection zone as well as to collect films. When the distance between the two plates is too small, the films obtained are not homogeneous because the high temperature is responsible for destroying SWNTs at the arc region, whereas the plates with a large distance cannot effectively collect samples. The optimal distance was found to be 40 mm in our experimental setup.

The thickness of the SWNT film can be controlled by changing the arc evaporation time. Under typical synthesis conditions, to get 150 nm thick films, the evaporation time was fixed at 1 min. Compared with the other growth methods; arc discharge is a relatively quick process. The size of as-synthesized films (Figure 1b) is almost the same as that of the graphite plate (diameter, 150 mm). A piece of as-grown film with a thickness of 150 nm is sliced, and the SEM image is shown in Figure 1c. This image indicates that the films are composed of the layers of the continuous sparse network in which long SWNT bundles are entangled with each other. At the junctions of bundles, some metal particles have been observed.

In our experimental setup, another important key point is the selection of catalyst and gas atmosphere. In comparison, we have tried to synthesize films using Ni/Y catalysts under He atmosphere with a pressure of 500 Torr.[20] Under this condition, a lot of flocklike structures were formed and floated in the chamber during arc discharge. After evaporation, the films have been deposited on the graphite plate, but the films are too flimsy to collect. In this case, only very thick films can be peeled off. In contrast, using Fe catalyst under a mixture of H_2 and Ar guarantees that the films produced in arc discharge are strong and long enough to transfer from one substrate to another.[19] The probable reason could be that the long time activity of Fe catalyst particles in this growth condition can give rise to long aspect ratio SWNT bundles, resulting in homogeneous strong film morphology. However, the Ni/Y could not sustain long time activity due to strong carbon coating, which leads to a shorter SWNT outcome. This observation is quite evident in our TEM analysis (not shown here).

Figure 2 shows the Raman spectra of SWNT films. In Raman spectra, we can get three characteristic vibration modes of SWNTs: the low-frequency radial breathing mode (RBM, 100−400 cm^{-1}), the high-frequency tangential mode around 1590 cm^{-1} (G-band), and the D-band around 1350 cm^{-1}. As shown in Figure 2a, three kinds of lasers with wavelengths of 514, 633, and 785 nm have been used to identify the diameters as well as metallic versus semiconducting SWNT distribution in our samples. Since the SWNTs' diameter is inversely proportional to the peak position in the RBM range, it can be calculated based on the equation, $d = 234/(\omega - 10)$, in which the RBM peak frequency is ω (cm^{-1}) and tube diameter is d (nm).[21] Consequently, we get the diameter distribution of as-grown samples, which lies in 0.9−1.9 nm, as shown in Figure 2a. In addition, peaks in the RBM range (514 nm: 195 cm^{-1}, 273 cm^{-1}; 633 nm: 147 cm^{-1}, 199 cm^{-1}; 785 nm: 146 cm^{-1}, 199 cm^{-1}, 226 cm^{-1}) can be assigned as metallic tubes, and

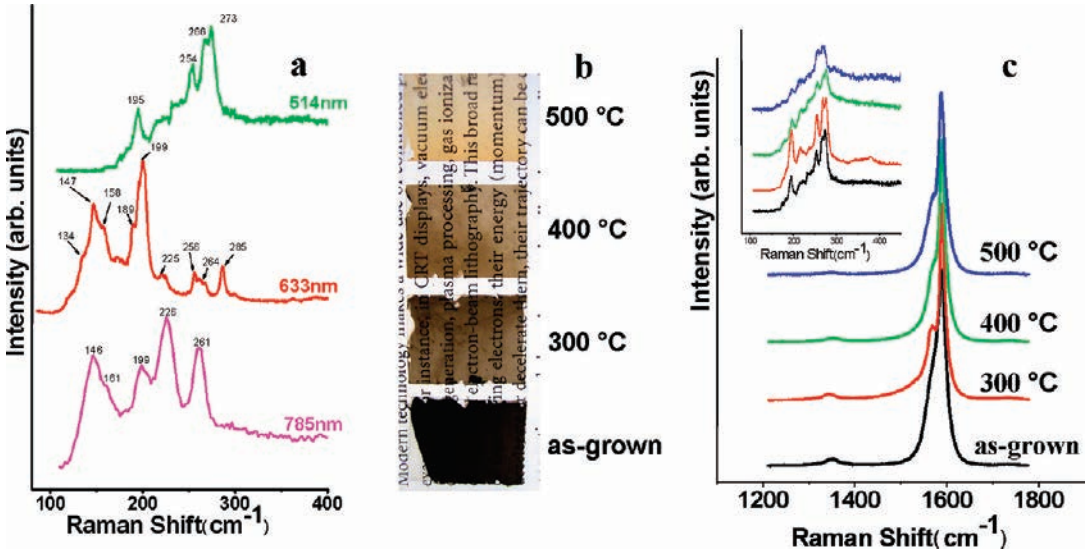

Figure 2. (a) Raman spectra (514, 633, and 785 nm) of as-grown sample in the RBM range. (b) The colors and transmittance changes induced by heat treatment under various temperatures. (c) Raman spectra (514 nm) changes brought by oxidation under various temperatures.

the rest of the peaks may come from semiconducting ones.[22] We also evaluate the effects of heat treatment on the SWNT films. The as-grown films are transferred to glass substrates and kept under various temperatures (300, 400, and 500 °C) for 1 h in open air. As indicated in Figure 2b, the oxidation processes have changed the transmittance as well as the colors of films. With the increase of oxidation temperature, the transmittance has been gradually improved, which may originate from the removal of amorphous carbon and defective SWNTs under higher temperature. Simultaneously, the colors of the film have been changed to pale yellow because Fe nanoparticles oxidized to Fe oxide during the aerial oxidation process. Figure 2b is an intuitive image that shows how the macroscopic films are affected by heat treatment. Detailed Raman analysis upon the heat treatment of the films is shown in Figure 2c. The RBM peaks have not disappeared or shifted even after 500 °C heat treatment. It implies that this process cannot selectively burn out SWNTs with specific diameters because the diameter distributions have not changed before and after oxidation. The D-band is regarded as originating from amorphous carbon or defects on the SWNTs' framework.[23] It significantly decreases with the increase of oxidation temperature and almost disappears when heating temperature reaches to 500 °C, as shown in Figure 2c. The intensity ratio (I_G/I_D) between G-band (I_G) and D-band (I_D) can comprehensively reflect the purity, crystallinity, and structural integrity of SWNTs, which is commonly used to evaluate their qualities. This value has been gradually increased from 24 for as-grown films to almost 70 for 500 °C heat-treated samples. The Raman analysis confirms the assumption mentioned earlier that the oxidation process could effectively remove the amorphous carbon as well as the defective SWNTs from as-grown samples. Moreover, the oxidation process effectively improved the transmittance of SWNT film, which is quite evident from Figure 2b.

Figure 3 shows TEM images of the SWNT films before purification, after oxidation under different temperatures, and after additional HCl treatment. The as-grown films present as entangled SWNT bundles with catalysts (~10 nm) attached on the surface appearing as the black dots (Figure 3a). After the oxidation process at 300 °C, some of the metal nanoparticles become larger in size due to the removal of amorphous carbon coating, followed by the agglomeration of Fe nanoparticles (Figure 3b). At 400 °C heat treatment, almost all amorphous carbon has been removed and the sidewalls of SWNTs get more clear (Figure 3c). Later, when we perform additional HCl treatment for 24 h, the effects of oxidation temperature on purification become quite prominent, shown in Figure 3d,e. Some nanoparticles and empty carbon cages are present in the samples after 300 °C oxidation, followed by HCl treatment (Figure 3d). However, 400 °C heat treatment accompanied with HCl rinsing successfully removes almost all the impurities (Figure 3e). According to the TG analyses on as-grown films, the maximum weight loss occurs at around 480 °C. Although the higher temperature oxidation process can remove more amorphous carbon and defective SWNTs, simultaneously, the majority of as-grown films can be oxidized at 500 °C. On the basis of the overall consideration of various factors, the appropriate temperature to perform heat treatment has been decided to be 400 °C, at which coated amorphous carbon on catalysts can be effectively removed without destroying the film network. As shown in Figure 3e,f, the low- and high-resolution TEM images of our purified samples confirm that this purification process can effectively remove impurities, which leads to a very clear SWNT network structure. Moreover, the HRTEM observations also indicate that the main product in our samples is SWNTs with diameters around 2 nm.

After a two-step purification process, the films were transferred onto quartz substrates to measure their transmittance. Figure 4a shows the consistent relationship between the thickness of film and the transmittance through UV−vis spectrometry. Under our experimental conditions, the film with a thickness of 30 nm is the thinnest one that we have achieved so far (Figure 4b, inset), where the transmittance reaches to 88% in the visible range. In the case of the 150 nm thick film, the transmittance is measured to be 77%. Moreover, the film with a thickness of 600 nm shows 20% transmittance.

The relationship between the sheet resistance and thickness is shown in Figure 4b. To compare our result with recently reported data, the electrical conductivity (σ) is calculated by $\sigma = 1/R_s t$ in which R_s is the sheet resistance and t is the thickness of the film.[24] The conductivity of film that is 30 nm thick is 1960 S/cm, which is comparable with the highest reported results in transparent films.[17] Moreover, it is suggested that our result is 2.7 times higher than that of solution-based arc discharge grown SWNT films.[10] In-depth analysis compared with as-reported results reveals that our technique is one of the best

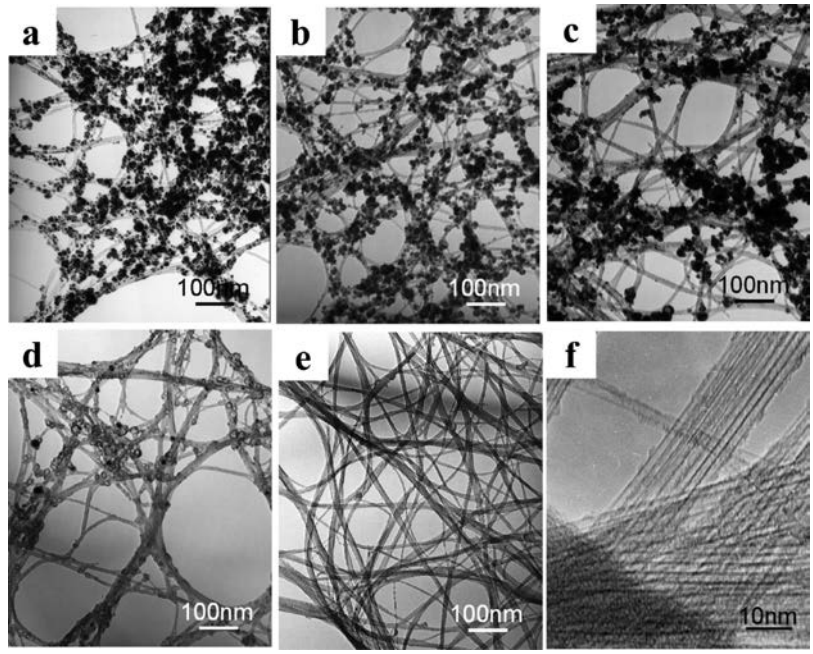

Figure 3. TEM observations during the purification process: (a) as-grown film; (b) film after 300 °C oxidization; (c) film after 400 °C oxidization; (d) film after 300 °C oxidization, followed by HCl treatment; (e) film after 400 °C oxidization, followed by HCl treatment. (f) HRTEM image of purified film.

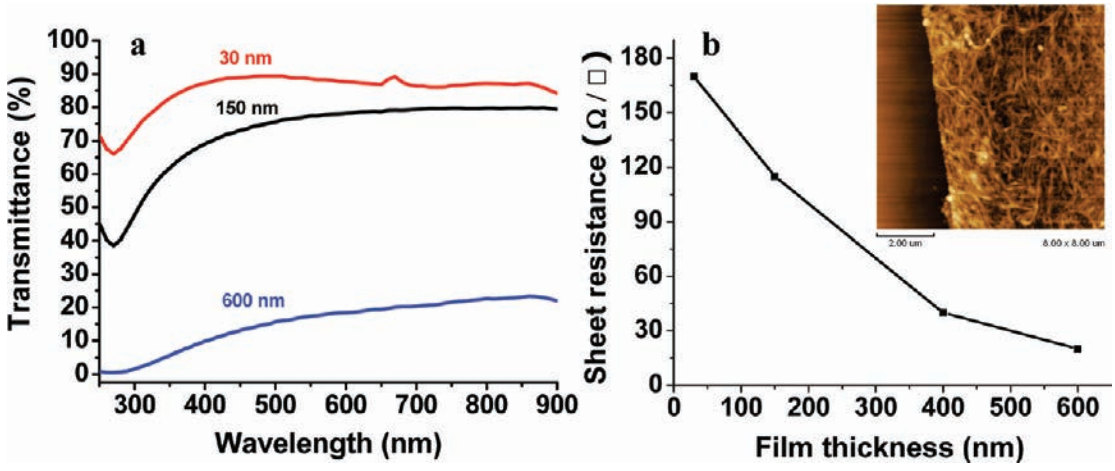

Figure 4. (a) Transmittance spectra of films with different thicknesses (30, 150, and 600 nm) in the visible range. (b) The correlation between the film thickness and the sheet resistance. Inset: SPM image of film with a thickness of 30 nm.

ways to synthesize highly transparent continuous SWNT networks within the smallest span of time of ~1 min. Wu et al.[15] have shown the transmittance of 50 nm film is 70%, whereas Ma et al.[17] can reach the highest level of transmittance up to 70% for the 100 nm film with a sheet resistance of 50 Ω/□, which is the best that has ever been reported. In contrast, for our homogeneous continuous purified SWNT network, the sheet resistance of 150 nm thick film is 117 Ω/□ with a visible light transmittance of ~77%.

Because the films are assembled by random SWNT bundles, many factors, including the purity, crystallinity, tube−tube interfaces, composition of metallic versus semiconducting SWNTs, and length of individual tubes, affect the overall conductivity. Until now, several methods have been developed to improve the conductivity of SWNT films.[25−27] According to the results of Hersam et al.,[25] compared with films using unsorted SWNTs, the conductivity of films with primary metallic tubes has been dramatically increased by 5.6 times in the visible range and 10 times in the infrared range. The controllable optical properties of the films have also been realized by accurate adjustment of the diameter of the metallic tubes. In our case, the metallic and semiconducting tubes coexist simultaneously, in which a considerable amount of metallic tubes have been identified by Raman analyses. The obvious absorption peak in the UV−vis spectra (shown in the Supporting Information) at 810 nm may mainly come from the first-order metallic transition of SWNTs with diameters of about 1.5 nm.[25] These analyses suggest that many metallic tubes are present in the films, which has effectively decreased the resistance of our SWNT films. Since the tube−tube interface is also a quite important factor in governing the conductivity, improving the contacts between tubes or increasing the length of tubes has been proved to promote the conductivity of the films.[26,27] On the basis of our experimental results, the good conductivity of the films is also due to the long SWNTs with high crystallinity obtained by this arc method. For our directly grown films, the SWNT bundles are firmly connected with each other during the growth process to form a continuous web structure. This leads to better contacts

and effectively lowers the tube−tube barrier resistance. Also, ultrasonication treatment that can effectively shorten the tube length is absent in our purification process. Only heating followed by HCl treatment on films will not damage the continuous network structure, as confirmed by the SPM observation (Figure 4b, inset); the purified films are assembled by long SWNT bundles. Although the arc-grown films contain the semiconducting as well as metallic SWNTs, in fact, the purification process has densified their network structures in which the overall conductivities are governed by the metallic tubes as well as the tube−tube resistance. In purified films, the metallic tubes can provide appreciable carriers for conduction; the densification effect of purification lowers the contact between the tubes, which will increase the degree of carrier delocalization so as to further improve the conductivity of the films.[26] As a result, we can obtain these highly conductive SWNT films by the arc discharge technique under our experimental condition.

The field emission performance of as-grown and purified (400 °C and HCl treatment) films is shown in Figure 5. The films are both pasted on the quartz surface and directly used as a cathode of field emission without further treatment. The as-grown film shows a very good field emission characteristic with the turn-on (E_{to} = 0.4 V/μm) and threshold fields (E_{th} = 1.4 V/μm) corresponding to the emission current density of 0.1 μA/cm^2 and 1 mA/cm^2, whereas the purified sample shows the corresponding turn-on and threshold fields as 0.6 and 1.7 V/μm, respectively. The calculation of the enhancement factor (β) is based on the Fowler−Nordheim (F−N) equation[28]

$$J = \frac{1.56 \times 10^{-6}\beta^2 E^2}{\Phi}\exp\left(-\frac{6.83 \times 10^9 \Phi^{3/2}}{\beta E}\right)$$

In this formula, J is the emission current density, Φ is the work function of SWNTs, β is the emission enhancement factor, and E is the average applied electric field. The corresponding β value can be extracted from the linear the plot of $\ln(J/E^2)$ versus $1/E$ from the above-mentioned equation as $\beta = 6.83 \times 10^9\Phi^{3/2}/(\text{slope} \times 10^6)$. We consider the work function (Φ) of SWNTs is 5.0 eV.[29] The field emission enhancement factor was calculated at two phases of applied potential, shown in the inset of Figure 5. At the high applied field, the corresponding values for as-grown and purified films were calculated to be 102 800 and 10 300, whereas low applied potential gives rise to the β values of 5500 and 2500.

It is well evident that the field emission properties are affected by various factors, including the CNT type, morphology of CNTs, fabrication method, and the experimental conditions. Hence, the exact comparison of field emission efficiency with as-reported results is hard, although our results are quite comparable with or at a higher end of those in recent reports.[29−31] Usually, the SWNTs were pasted on the conductive coatings, such as Ti, Cr, and Ag/Ti, to form an ohmic contact between SWNTs and substrates, which proved to enhance the field emission properties to a certain extent.[31,32] In our technique, no such type of conductive coating is required. The films on quartz surface were directly used as cathodes without further treatment, where the film itself is acting as a good conductor as well as an effective emitter, which shows a quite low turn-on and threshold voltage.

In fact, as-synthesized film consists of a horizontal homogeneous CNT network attached with tiny Fe nanoparticles as well as defective SWNTs. We believe this homogeneous CNT network can act as a good conductor, whereas the nanoparticles and defective SWNTs are acting as the emitter sites that could

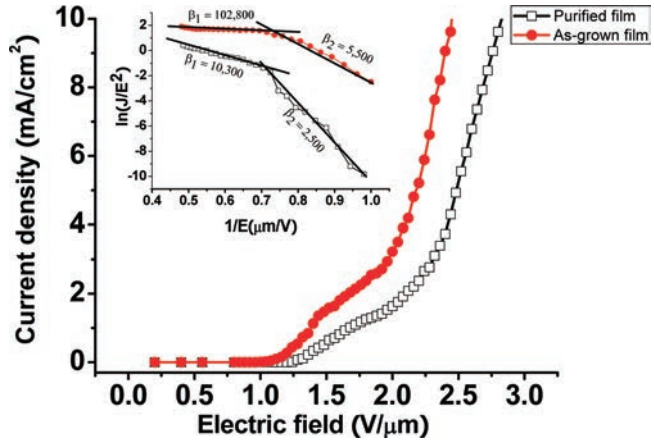

Figure 5. Field emission from purified and as-grown SWNT films. Inset: the corresponding Fowler−Nordheim plots. For unpurified films, the two phases' β values are calculated to be 102 800 and 5500. For purified films the β values are 10 300 and 2500.

successfully enhance the emission performance.[33] Moreover, after purification, it was observed that the emission performance of films decreases quite effectively due to the removal of a significant amount of active emitter sites.

In summary, our study shows a controllable growth of semitransparent continuous SWNT films with the smallest period of time. The unique homogeneous network structure due to strong interlinking between the tube bundles in the as-synthesized films is likely to have diverse potential gradient in various sophisticated device technologies, such as touch panels, sensors, flexible displays, etc. In our study, the effective removal of impurities can enhance the transmittance as well as the conductivity to a certain extent. The purified film of high conductivity with comparable transparency could be a suitable complement for ITO coating. The experimental result shows that the transferable as-grown films possess better field emission performance, which could be easily scaled up to large area homogeneous films for field emission display in the near future.

Acknowledgment. We thank Professor M. Hiramatsu of Meijo University for allowing us to use the Raman spectrometer. We are also thankful for the support from the 21st Century COE Program of the Ministry of Education, Culture, Sports, Science and Technology, Japan. We are grateful to Mr. T. Ueda and Mrs. M. Saito of the Institute of Molecular Science (IMS), Okazaki, for providing the UV−vis facility. A part of this study was supported by the Joint Studies Program (2008) of the IMS.

Supporting Information Available: Absorption spectrum of SWNT film. This material is available free of charge via the Internet at http://pubs.acs.org.

References and Notes

(1) Dresselhaus, M. S.; Dresselhaus, G.; Avouris, P. *Carbon Nanotubes: Synthesis, Structure, Properties and Applications*; Springer: New York, 2001.
(2) Martel, R.; Schmidt, T.; Shea, H. R.; Hertel, T.; Avouris, P. *Appl. Phys. Lett.* **1998**, *73*, 2447.
(3) Tans, S. J.; Verschueren, A. R. M.; Dekker, C. *Nature* **1998**, *393*, 49.
(4) Kong, J.; Franklin, N. R.; Zhou, C.; Chapline, M. G.; Peng, S.; Cho, K.; Dai, H. *Science* **2000**, *287*, 622.
(5) Ismach, A.; Kantorovich, D.; Joselevich, E. *J. Am. Chem. Soc.* **2005**, *127*, 11554.
(6) Han, S.; Liu, X.; Zhou, C. *J. Am. Chem. Soc.* **2005**, *127*, 5294.
(7) Grüner, G. *J. Mater. Chem.* **2006**, *16*, 3533.

(8) Novak, J. P.; Snow, E. S.; Houser, E. J.; Park, D.; Stepnowski, J. L.; McGill, R. A. *Appl. Phys. Lett.* **2003**, *83*, 4026.

(9) Zhang, M.; Fang, S.; Zakhidov, A. A.; Lee, S. B.; Aliev, A. E.; Williams, C. D.; Atkinson, K. R.; Baughman, R. H. *Science* **2005**, *309*, 1215.

(10) Zhang, D.; Ryu, K.; Liu, X.; Polikarpov, E.; Ly, J.; Tompson, M. E.; Zhou, C. *Nano Lett.* **2006**, *6*, 1880.

(11) Guo, P. S.; Chen, T.; Chen, Y. W.; Zhang, Z. J.; Feng, T.; Wang, L. L.; Lin, L. F.; Sun, Z.; Zheng, Z. H. *Solid-State Electron.* **2008**, *52*, 877.

(12) Sreekumar, T. V.; Liu, T.; Kumar, S.; Ericson, L. M.; Hauge, R. H.; Smalley, R. E. *Chem. Mater.* **2003**, *15*, 175.

(13) Armitage, N. P.; Gabriel, J. C. P.; Grüner, G. *J. Appl. Phys.* **2003**, *95*, 3228.

(14) Meitl, M. A.; Zhou, Y.; Gaur, A.; Jeon, S.; Usrey, M. L.; Strano, M. S.; Rogers, J. A. *Nano Lett.* **2004**, *4*, 1643.

(15) Wu, Z.; Chen, Z.; Du, X.; Logan, J. M.; Sippel, J.; Nikolou, M.; Kamaras, K.; Reynolds, J. R.; Tanner, D. B.; Hebard, A. F.; Rinzler, A. G. *Science* **2004**, *305*, 1273.

(16) Hu, L.; Hecht, D. S.; Grüner, G. *Nano Lett.* **2004**, *4*, 2513.

(17) Ma, W.; Song, L.; Yang, R.; Zhang, T.; Zhao, Y.; Sun, L.; Ren, Y.; Liu, D.; Liu, L.; Shen, J.; Zhang, Z.; Xiang, Y.; Zhou, W.; Xie, S. *Nano Lett.* **2007**, *7*, 2307.

(18) Nikolaev, P.; Bronikowski, M. J.; Bradley, R. K.; Rohmund, F.; Colbert, D. T.; Smith, K. A.; Smalley, R. E. *Chem. Phys. Lett.* **1999**, *313*, 91.

(19) Zhao, X.; Inoue, S.; Jinno, M.; Suzuki, T.; Ando, Y. *Chem. Phys. Lett.* **2003**, *373*, 266.

(20) Journet, C.; Maser, W. K.; Bernier, P.; Loiseau, A.; Lamy de la Chapelle, M.; Lefrant, S.; Deniard, P.; Lee, R.; Fischer, J. E. *Nature* **1997**, *388*, 756.

(21) Milnera, M.; Kürti, J.; Hulman, M.; Kuzmany, H. *Phys. Rev. Lett.* **2000**, *84*, 1324.

(22) Maultzsch, J.; Telg, H.; Reich, S.; Thomsen, C. *Phys. Rev. B* **2005**, *72*, 205438.

(23) Ferrari, A. C.; Robertson, J. *Phys. Rev. B* **2000**, *61*, 14095.

(24) Bekyarova, E.; Itkis, M. E.; Cabrera, N.; Zhao, B.; Yu, A.; Gao, J.; Haddon, R. C. *J. Am. Chem. Soc.* **2005**, *127*, 5990.

(25) Green, A. A.; Hersam, M. C. *Nano Lett.* **2008**, *8*, 1417.

(26) Blackburn, J. L.; Barnes, T. M.; Beard, M. C.; Kim, Y. H.; Tenent, R. C.; McDonald, T. J.; To, B.; Coutts, T. J.; Heben, M. J. *ACS Nano* **2008**, *2*, 1266.

(27) Simien, D.; Fagan, J. A.; Luo, W.; Douglas, J. F.; Migler, K.; Obrzut, J. *ACS Nano* **2008**, *2*, 1879.

(28) Fowler, R. H.; Nordheim, L. W. *Proc. R. Soc. A* **1928**, *119*, 173.

(29) Ha, B.; Park, J.; Kim, S. Y.; Lee, C. J. *J. Phys. Chem. B* **2006**, *110*, 23742.

(30) Zhang, H.; Shin, D. H.; Lee, H. S.; Lee, C. J. *J. Phys. Chem. C* **2007**, *111*, 12954.

(31) Wei, Y.; Weng, D.; Yang, Y.; Zhang, X.; Jiang, K.; Liu, L.; Fan, S. *Appl. Phys. Lett.* **2006**, *89*, 063101.

(32) Zhang, J.; Wang, X.; Yang, W.; Yu, W.; Feng, T.; Li, Q.; Liu, X.; Yang, C. *Carbon* **2006**, *44*, 418.

(33) Kumar, M.; Okazaki, T.; Hiramatsu, M.; Ando, Y. *Carbon* **2007**, *45*, 1899.

JP8114463